IDETC2019-97163

A NOVEL AUTONOMOUS SCALED ELECTRIC COMBAT VEHICLE

Aaron Hao Tan
University of Ontario Institute of
Technology
Oshawa, Ontario, Canada

Haoxiang Lang
University of Ontario Institute of
Technology
Oshawa, Ontario, Canada

Moustafa El-Gindy
University of Ontario Institute of
Technology
Oshawa, Ontario, Canada

ABSTRACT

Current literature pertaining to multi-steerable mobile platforms and the progression of military vehicles in the past few decades suggest a lack of effort in pursuing advanced technologies in this joint area. As a result, a novel 1:6 scaled electric combat vehicle prototype that features eight independently driven and steerable wheels is designed and developed in this paper. The intent is to create a scaled model for future autonomous vehicle navigation and control research in off road terrains. Starting with the mechanical design, this paper discusses the details of the chassis, suspension, driving and steering systems development. The electronics necessary for vehicle actuation is implemented with custom nodes and topics created for hardware communication within the Robot Operating System (ROS). Lastly, path planning and obstacle avoidance abilities are implemented to achieve autonomous navigation. The result of this work is a fully functional and instrumented robotic platform with a modular software architecture. Vehicle design analysis, performance and autonomous navigation abilities are experimentally tested with promising results.

INTRODUCTION

Because of its ability to maneuver in rough terrains, multi-wheeled vehicles often find their applications in off-road environments that range from agriculture and military to space exploration. In this work, the primary application is military based with a focus on the Light Armored Vehicles (LAV) designed by General Dynamics Land Systems in Canada [1]. This type of vehicles finds its principal applications in civil law enforcement and personnel transportation. Throughout its history, there have been several iterations to this family of vehicles which all share the same eight wheeled design and front wheel steering. The first member of the LAV family dates to 1983 with the release of the LAV-25 [2] which featured an amphibious design. In 1999, an updated design known as the LAV III was released with new features such as a height management system, central tire inflation system and improvements in maximum payload capacity and protection [3] [4]. This vehicle was in service for the next 16 years until 2015 when the government of Canada decided to upgrade all LAV III's by implementing several new features. The renovated models are known as the LAV 6.0 and it featured an upgraded suspension system, higher horse power engine, better protection and a complete switch to digital electronic systems within the vehicle [5]. LAV 6.0 entered service in 2015 and are expected to remain in duty until 2035. Currently, a new LAV model known as the LAV 700 (Fig. 1), is scheduled to enter production [6]. This vehicle features an improved control architecture when compared to LAV 6.0 and boasts other innovative features such as self-sealing fuel tanks, modular protection system and other advancements in engine horsepower. From the mentioned designs, it is evident that the primary improvements made to the LAV since the 80's have been centered around engine output and passenger protection with a lack of effort in implementing autonomous navigation and multi-steered features. This is further supported by scarce publications relating to this topic.

In order to provide a more in-depth review relating to autonomous multi-steered systems that mimic the design of the LAV, an alternative approach is to survey the field of mobile robotics due to shared fundamentals with autonomous vehicle research. Furthermore, an added benefit of this is mobile robots are more accessible than fully instrumented vehicles; therefore, there are significantly more publications available involving the design and development of multi-steered and multi-axle platforms with autonomous abilities. Starting with multi-axle designs such as the six wheeled prototypes that feature rocker bogie suspensions proposed in [7-9] for aerospace applications. Although the authors from these works proposed multi-wheeled designs, these platforms utilize differential steering as the main maneuvering approach which is contrary to what is employed by the LAV. To explore literature surrounding independently steered Ackermann systems, the authors in [7] created a four-wheel drive and four-wheel steer (4WD4WS) prototype with applications in data collection for agriculture usage. In [8], a similar 4WD4WS

is equipped with a fuzzy logic controller for autonomous navigation of unexplored environments. Another platform with independently driven and steerable wheels is presented in [9] where applications in lane following and parking using machine vision is presented. This work features a series of cameras while the authors in [10] proposed a single camera system for autonomous steering. Other navigation work for 4WD4WS platforms are proposed in [11] [12]. From the mentioned publications, independently steered platforms are centered around two axle configurations while designs with more wheels are limited. Multi-axle and multi steered research are primarily focused on simulation-based results with a lack of physical implementation and validation. For example, the authors in [13] worked on motion control of a six wheel drive and six wheel steer (6WD6WS) platform to improve its maneuverability while the dynamic model, controllability and stability of a similar platform are analyzed in [14] and [15]. As for work published for eight wheeled combat vehicle designs, [16] proposes an optimal path planning algorithm that uses artificial potential field. A side slip controller that takes advantage of the third and fourth axle of the LAV is proposed in [17] while a heading angle controller using H-infinity is proposed in [18].

Based on the reviewed literature, a scaled robotic platform that features a multi-steerable system while mimicking the design of multi-wheeled combat vehicles is necessary to advance autonomous navigation research in the military field. Such a system would be advantageous in the development of vehicle control, path planning and other intelligent algorithms for off road terrains and cluttered environments. At the time of writing, the described platform is not available in the commercial space as well as relevant publications as they focus on robots equipped with two axles, differential steer and no suspension. As a result, completion of an electric multi-axle and multi-steered robotic platform will not only represent a possible future combat vehicle design, it will also bring experimental validation to an area dominated by simulation-based publications. Motivated by this reason, the following will cover the mechanical, electrical and software architecture design of a novel 8x8 scaled electric combat vehicle (SECV) that is capable of multiple steering configurations. In addition, the final product features both path planning and obstacle avoidance abilities. Vehicle performance and navigation capabilities are evaluated with physical experiments in the following paper.

FIGURE 1. LAV 700 [6]

DESIGN REQUIREMENTS

In this section, the design requirements for the proposed SECV are presented. Starting with the dimension, a typical multi-wheeled combat vehicle is approximately 7 meters long, 2.7 meters wide and 2.8 meters tall with a tire radius of 0.545 meter [19]. These dimensions and the weight are divided by 6 and 6^3, respectively, to meet the 1:6 ratio target. In addition, the prototype must be able to overcome obstacles of minimum 0.1 meter for rough terrain navigation research; therefore, a double wishbone suspension design is required for its large travel with no camber change. Furthermore, the chassis must be designed accordingly because of the suspension's space conscious nature. In terms of vehicle motion, independent actuation is required to allow future users with the freedom to control each wheel individually for the development of vehicle dynamics algorithms such as torque vectoring, traction control...etc. Since the maximum velocity of a typical combat vehicle is 100 km/h, the scaled speed should theoretically be 16.67 km/h. However, this speed is too high for safe operations; as a result, only half is required to be two times faster than commercial mobile robots of similar size and weight [20]. In terms of steering, the SECV must feature independent actuators to achieve multi-steerable configurations. The maximum steering angle must be 35 degrees with less than 1 degree of tolerance in steering accuracy. Furthermore, lock to lock time of less than 1.5 seconds is desired to ensure responsive steering performance. Aside from actuation and form factor, the SECV must feature range and image sensors for autonomous navigation research. This will include a central computing unit connected with sensors that are able to acquire wheel speed, acceleration, steering and heading angles. The operation time of the vehicle must be at least 2 hours on a single charge with swappable batteries for additional time. Most importantly, there are no value in a design that cannot be made, assembled or unreasonably costly to produce; therefore, Design for Excellence is considered throughout the development of the SECV [21]. This include design considerations such as parts with flat bases to allow proper adhering to heating beds and easy clamping and referencing for 3D printing and CNC milling, respectively. The following table tabulates key requirements of the proposed SECV.

Table 1 Scaled Vehicle Design Requirements

Area	Requirements
Dimension & Weight	1.16m x 0.45m x 0.42m at 84 kg
Suspension	Double wishbone setup
	Travel: 0.1m
Steering	Max angle: 35 degree (< 1 deg tol.)
	Lock to lock time: <1.5 s
Driving	Max speed: 8.3 km/h
	Wheel radius: 0.09 m
Sensors	Range Sensor
	Camera
	Wheel Encoder
	Steering angle
	Inertial Measurement Unit

THE SCALED ELECTRIC COMBAT VEHICLE

With the design requirements set, the mechanical design as well as the electronics and software architecture of the proposed SECV prototype is presented in this section. Starting with the mechanical design of the SECV which is classified in to four different subsystems; namely, suspension, chassis, driving and steering. Additionally, a detailed hardware architecture of all electronics including sensors, actuators and controllers is presented. This discussion will lead in to preparing the SECV for autonomous navigation by implementing the Robot Operating System within the vehicle. By doing so, a software environment is available for research and development. Lastly, a model is derived to describe the kinematics and steering geometry of the vehicle.

Mechanical Design

The following sub sections will discuss the details regarding the suspension, chassis, driving and steering systems.

A. Suspension Design

Beginning with the suspension as it is critical in dictating the design of the chassis which consequently determines the driving and steering system design. As mentioned in the requirements, a double wishbone setup is implemented where the steering knuckle is mounted on two "control arms"; an upper arm and a lower arm as seen in Fig. 2 which illustrates the front view of the SECV's CAD model. The advantage of using a double wishbone is because of its allowance for large wheel travel, which is advantageous in all-terrain vehicles. In terms of manufacturing, the suspension system is made of mostly standard parts except for the lower control arm which is water jet cut to reduce the mass of the part while retaining rigidity. A channel is milled along the top to accommodate the output axle and the holes for mounting while shocks are mirrored across the control arms to create an interchangeable part. Based on the required suspension travel of 0.1 meter, the lengths of the control arms are designed accordingly to remain parallel to each other while the angle of the arms changes. The goal is to keep the tires at their set camber throughout the suspension travel to increase handling. In order to select the appropriate ratings for the shock absorbers, the SECV is assumed to be symmetrical with the center of gravity (CG) located in the middle of the chassis. In this case, the normal force at each wheel, F_{norm}, is approximately 102 N based on even distribution of the desired vehicle weight. Consequently, the required strength for each shock absorber, F_{shocks}, is calculated at full compression to be approximately 142.4 N based on the force geometry (blue) shown in Fig. 2. With this in mind, 178 N shocks are chosen to provide a safety factor of 1.25.

$$F_{Norm} = m_{per\ wheel} * g = 102\ N \qquad (1)$$

$$F_{shocks} = F_{norm} * \cos(\emptyset) = 142.4\ N \qquad (2)$$

B. Chassis Design

Bounded by the dimension and weight requirement, the design of the SECV chassis is made of aluminum and it resembles the letter *T* as it conforms to the suspension setup. More specifically, the chassis is broken down into seven aluminum pieces which include: two identical left and right-side panels, two identical front and back pieces. These seven aluminum pieces are water jet cut and bent with the side panels designed to be symmetrical to make the parts interchangeable; thereby improving cost and ease of assembly. Rivets are chosen as the method of connecting panels because of their ease of removal and strength. Within the chassis are three storage layers which hold the driving, steering and computing devices. These layers are designed to be the same dimensions with different mounting points required for each shelf. An additional support bolt is added to the steering layer as any movement to this shelf could cause damage to the steering components. With the design of the suspension and chassis in place, the dimensions of the SECV with the aesthetic shell are 1.13 meters long, 0.5 meters wide and 0.45 meters tall which yields an acceptable error when compared with the design requirements. Fig 3 shows an aesthetic enclosure which sits on top of the chassis to mimic the overall profile of a typical multi-wheeled combat vehicle.
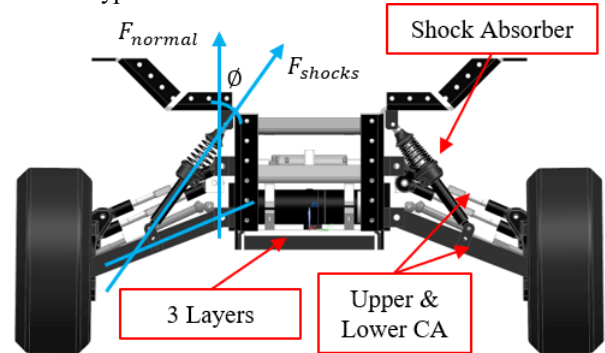

FIGURE 2. Front View of SECV

FIGURE 3. The Scaled Electric Combat Vehicle Prototype

C. Driving Layer (Bottom Layer)

With the overall form factor of the SECV in place, the next task is to meet the driving requirements. To achieve the desired top speed with the given dimension and weight of the vehicle, the motors are chosen based on the following torque

calculations. In this case, the static coefficient of adhesion between rubber tires and pavement for the wheel is 0.7 while the rolling resistance coefficient is assumed to be 0.02 [22] [23]. As a result, the following calculates the friction forces experienced at each wheel.

$$F_{friction} = F_{norm} * \mu_{static} = 72.1\,N \qquad (3)$$

$$F_{roll} = F_{norm} * \mu_{rolling} = 2.06\,N \qquad (4)$$

Considering the scaled radius of the wheel, the required torque is calculated as follows.

$$T_{required} = F_{friction} * R_{wheel} = 6.73\,Nm \qquad (5)$$

$$T_{roll\ required} = F_{roll} * R_{wheel} = 0.19\,Nm \qquad (6)$$

Based on these requirements, the following table summarizes the characteristics of the DC motors and gearbox implemented.

Table 2 Motor and Gearbox Specification

Category	Specifications
Nominal Current ($I_{nominal}$)	4A
Stall Torque (T_{stall})	929 mNm
Torque Constant (TC_{motor})	19.4 mNm/A
No Load Speed	7180 rpm
Gear Ratio (G_{ratio})	33:1

Using the information provided in Table 2, the nominal torque that the motor is capable of is calculated as follows.

$$T_{nominal} = TC_{motor} * I_{nominal} = 0.0776\,Nm \qquad (7)$$

With a 33:1 transmission, the following shows the supplied nominal and stall torque.

$$T_{nominal} = G_{ratio} * T_{motor} = 2.56\,Nm \qquad (8)$$

$$T_{stall} = G_{ratio} * T_{motor} = 30.66\,Nm \qquad (9)$$

With a stall torque of 30.66 Nm, this is more than enough to overcome the $T_{required}$ of 6.73 Nm. Once the vehicle gets moving, the nominal supplied torque is 2.56 Nm, which is also more than enough to overcome the $T_{roll\ required}$ of 0.19 Nm. Furthermore, the selected motors are able to output at 7180 RPM which is 217 RPM after the gearbox. With this output, the top speed of the SECV is approximately 7.64 km/h as calculated below. This yields an acceptable error of 7.95% when compared with the desired of 8.3 km/h.

$$v_{max} = \omega_{motor} * R_{wheel} * 3.6 = 7.64\,km/h \qquad (10)$$

Due to the constraint on chassis size, a custom pulley box is necessary to transfer the motor output to each wheel as shown in Fig. 4. To do this, two double flange pulleys are used to prevent misalignment and lateral movement of the belt. In addition, M4 set screws are applied to maintain torque between the input/output shafts and the pulleys. Each set screw has an approximate holding power (tangential force) of 712 N when torqued to 0.5 Nm [24]. A 30% increase in holding torque is obtained by using the second set screw [25]. A 712 N holding power can be converted to a working torque using the following calculation where the service factor allows the pulley box to operate with approximately 25% more torque before the set screws risk losing retention on the axles.

$$T_{operating} = D_{shaft} * P_{holding} = 4.27\,Nm$$
$$Service\ Factor \approx 1.25 \qquad (11)$$

In terms of the belts used in the pulley box, 3-millimeter pitch GT3 belts (Gates timing belts) in a 6-millimeter width are employed as the operating conditions lie within the operating range of the shaft speed (217 RPM) and designed torque capacity (6.73 Nm) as calculated previously. In addition, these belts also have a curvilinear tooth profile, which increases load carrying capacity over a traditional trapezoidal tooth design [26]. An added benefit of the pulley box design is that it accounts for an encoder mounting location between itself and the side wall of the chassis. Due to limited space within the chassis, this is the only place to mount the encoders. Next, constant velocity (CV) joints are used to transfer the pulley output to the axle which ultimately connects to the steering knuckle and wheel. In terms of CV joints, Rzeppa and the Bendix-Weiss joints are common in military designed vehicles [27]. Both the mentioned joints are ball bearing types, where the balls furnish the only points of driving contact between the two halves of the coupling. The increased number of points of contact in the joint between the two halves of the coupling decreases wear of the components and reduces vibration in the joint. In this design, Rzeppa joints are implemented as they can operate in the range of 45° to 48° of articulation.
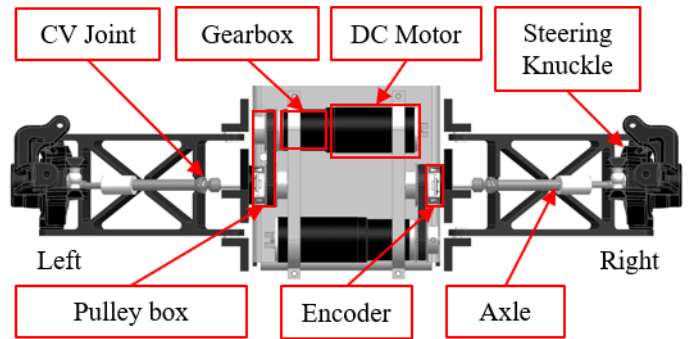

FIGURE 4. Top View of One Axle in Driving Layer

D. Steering Layer (Middle Layer)

The layer above the Driving Layer is the Steering Layer which is home to eight linear actuators for independently steerable wheels. The process for selecting the servo involved

determining the best option that would provide the required actuation force, steering response time and stroke to achieve desired steering angles. To begin, a stroke of 45 millimeter is determined to achieve the desirable maximum steering angle when considering the control arm and wheel assembly geometry. With the weight of the vehicle, it was estimated that an actuation force of 24.47N, would be required to steer each wheel in a "dry steering" situation based on physical experimentation. With the determined stroke requirement as well as steering response time, the selected servo must be able to extend and retract at a minimum speed of 30 mm/s as seen in the calculation below. It can be assumed that less force will be required to steer while the wheels are rotating.

$$V_{servo} = \frac{45mm}{1.5s} = 30 \ mm/s \qquad (12)$$

Using these requirements, the P16 series linear actuators by Actuonix are selected due to its peak efficiency point at 25N and 34 mm/s, not to mention the maximum force and speed of 50N and 46 mm/s, respectively [28]. Furthermore, these servos also feature built in potentiometers that will provide steering angle feedback. To fit within the suspension design, an offset coupler is necessary to connect the servos with the tie rod as seen in Fig. 5. The benefits of the linear actuator system are the structural rigidity and robustness that they offer. In other words, they reduce steering compliance by keeping the steering angle at the desired value even in the presence of disturbance forces up to 500N.
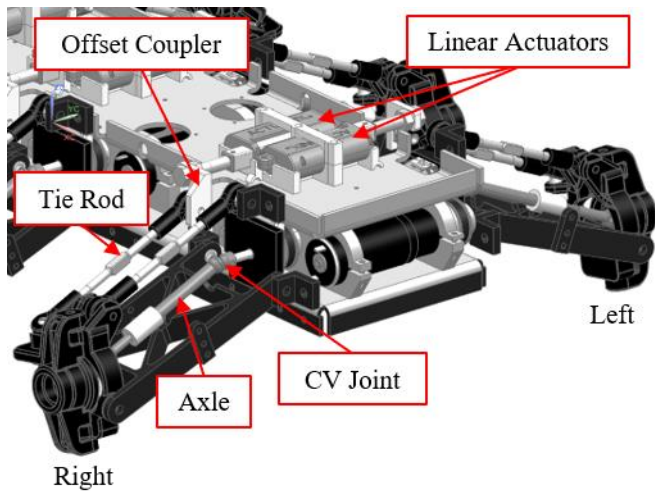

FIGURE 5. Isometric View of Steering Layer

Electronic Hardware Architecture

In this section, the required electronics to create an operational prototype are embedded within the SECV. These electronics include a central computing unit which is a laptop that features an Intel Core-i5 processor loaded with Ubuntu 14.04. This laptop acts as the brain of the SECV since it is where all the software files are stored and executed. Connected to the laptop are several peripherals which include a Bluetooth receiver, laser scanner, Inertial Measurement Unit (IMU), single lens camera, steering and motor controllers. The Bluetooth receiver is used for close range teleoperation as it receives commands from a wireless joystick controller. The laser, IMU and camera are used for autonomy applications with more details provided in later sections. The steering controller consists of an Arduino board with a motor controller shield attached. Each board is able to control up to four linear actuators; therefore, two steering controllers are necessary for the SECV. Besides drawing power from the onboard 12V supply and providing it to the actuators, the steering controllers are also responsible for receiving stroke position feedback from the built-in potentiometers to conduct closed loop control. On the other hand, each motor controller control two motors each with four in total embedded within the prototype. However, only a master controller is connected to the laptop via USB as the other three exist as slave nodes on a CAN network. Each motor controller receives power from the onboard 15V supply and subsequently delegates it to each DC motor as well as their respective encoders. The encoders provide feedback directly to the motor controller to create closed loop speed control. The described architecture is illustrated in the figure below.
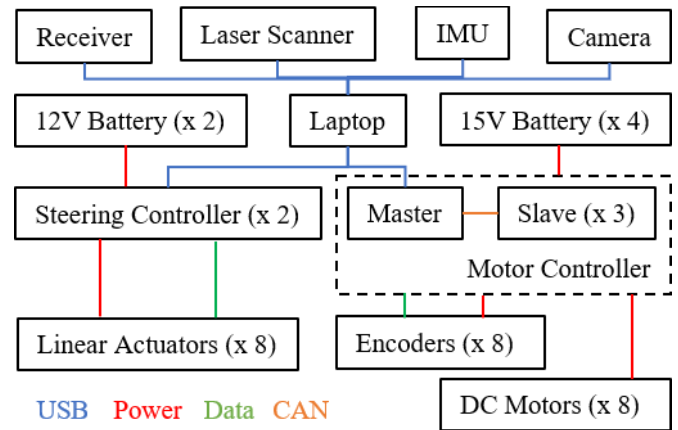

FIGURE 6. Electronic Hardware Architecture

Software Environment and Hardware Communication

In 2007, a framework known as Robot Operating System (ROS) was released to the public to create a standard platform for researchers and enthusiasts to develop complete robotic systems [29]. Since then, the operating system has received several updates to include newer features and better stability. Currently, ROS offers a variety of useful tools and libraries that helps with hardware abstraction and low-level device control. One of the main tools is its node-based network that enables hardware and software communication. In this network, each node represents either a hardware or software. Communication is achieved through publishing and subscribing to different topics that users may create. Each topic holds standardized message types as defined by ROS. In the following section, custom nodes and topics are created for all internal hardware of

the SECV to create a modular software environment. To begin, teleoperation for the SECV is first created to allow for user control. In this case, a /teleop node is written to publish to a topic called cmd_vel which includes both a linear and an angular velocity message. This topic is critical in controlling the motion of the SECV as any additional software tasked with motion control are to publish to this topic. For example, other navigation based software can be represented by the placeholder node called, *other_nav_nodes* in Fig. 7. As a safety measure, the /teleop node is always prioritized over any other nodes publishing to the cmd_vel topic as user commands should override control of the SECV during emergency situations. Moving forward, the linear velocity message within the cmd_vel topic is subscribed by the /motor_driver node which subsequently dictate the motor output. A /convert_to_ackermann node is created to subscribe to both the linear and angular velocity messages to calculate the appropriate steering angles based on Ackermann steering geometry. The steering angles are published and subscribed by the /steering_controller node which then controls the linear actuators. Besides motion control, nodes and topics are also written for the onboard sensors. For example, the /usb_camera node publishes to a topic called rgb_image which holds a matrix message representing the RGB values of each pixel to form an image. The laser, IMU and encoder nodes are responsible for publishing to topics such as laser_scan, yaw and lin_tran, respectively. These topics are available for subscription by any future nodes that may include navigation within ROS. The described network is illustrated in Fig. 7 where squares and ovals symbolize nodes and topics, respectivcely. It is important to note that this figure shows a simplified network for clarity purposes as there are more nodes that exist within the vehicle which handles other aspects such as feedback control, power manegement and background processes.
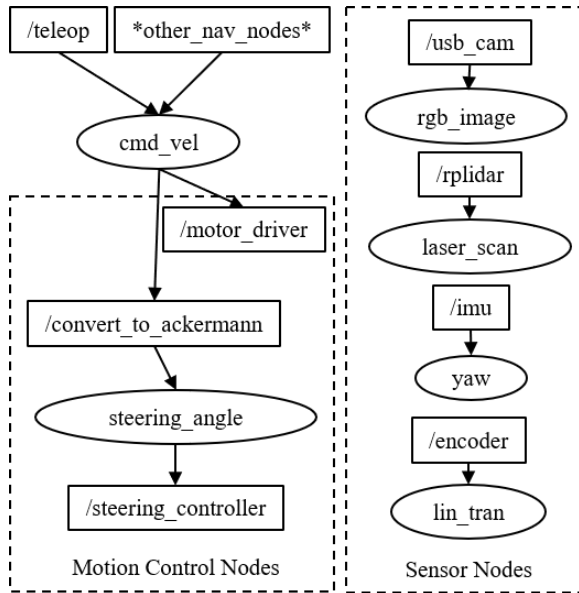

FIGURE 7. ROS Nodes and Topics

Ackermann Steering and Kinematics Model

In this section, the steering geometry and kinematics model of the SECV is described. According to Ackermann steering geometry, an instantaneous turning center is denoted as P in Fig. 8. This is the point at which lines perpendicular to the forward axis of each wheel must intersect during cornering maneuvers. The aim is to ensure that the wheels experience pure forward rolling motion without lateral forces that cause tire scrubbing. The following equations calculate the steering angles of each wheel which are denoted as $(\delta_{Li}, \delta_{Ri})$. These equations are based on similar triangles and trigonometry where the turning radius, R, is measured between the turning center and the CG of the vehicle. The track width and wheel base of the SECV is represented by t and l, respectively.

$$\begin{aligned} \delta_{L1} &= \tan^{-1}\left(\frac{l_1}{R - t/2}\right), \\ \delta_{R1} &= \tan^{-1}(\frac{l_1}{R + t/2}) \end{aligned} \tag{13a}$$

$$\begin{aligned} \delta_{L2} &= \tan^{-1}\left(\frac{l_2}{R - t/2}\right), \\ \delta_{R2} &= \tan^{-1}(\frac{l_2}{R + t/2}) \end{aligned} \tag{13b}$$

$$\begin{aligned} \delta_{L3} &= \tan^{-1}\left(\frac{l_3}{R - t/2}\right), \\ \delta_{R3} &= \tan^{-1}(\frac{l_3}{R + t/2}) \end{aligned} \tag{13c}$$

$$\begin{aligned} \delta_{L4} &= \tan^{-1}\left(\frac{l_4}{R - t/2}\right), \\ \delta_{R4} &= \tan^{-1}(\frac{l_4}{R + t/2}) \end{aligned} \tag{13d}$$

When compared to differential steered systems, car-like robots with Ackermann steering exhibit one extra state which is the steering velocity, $\dot{\varphi}$. In Fig. 8, the CG is assumed to be at the center of the vehicle and its location is denoted as (x, y). The heading angle, θ, is measured between the longitudinal axis of the SECV and the x-axis. Conversely, the steering angle is measured between the current linear velocity, v, and the longitudinal axis of the SECV. When describing the velocities with respect to the x and y axis, both angles are combined as shown in Eqn. 14 and 15. The angular velocity of the vehicle, $\dot{\theta}$, considers the linear velocity, total wheel base and the steering angle as presented in Eqn. 16.

$$\dot{x} = v\cos(\theta + \varphi) \tag{14}$$

$$\dot{y} = v\sin(\theta + \varphi) \tag{15}$$

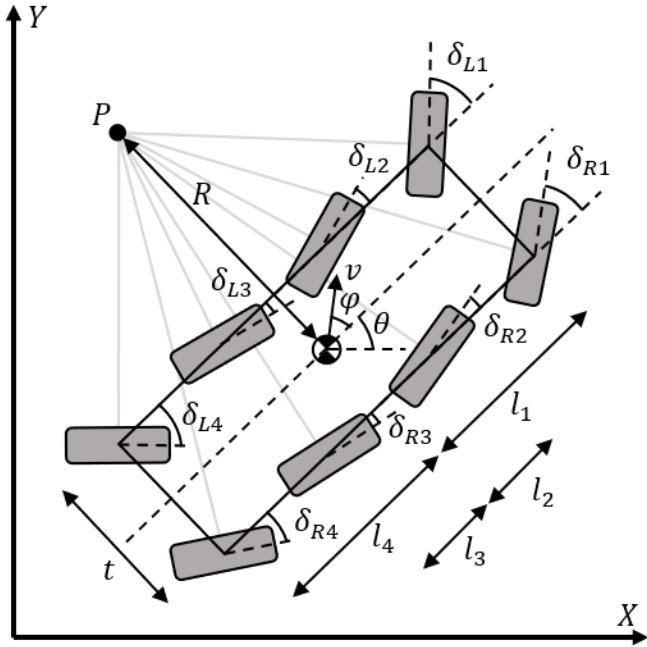$$\dot{\theta} = \frac{v}{l}\sin(\varphi) \tag{16}$$

FIGURE 8. Kinematics Model of SECV

AUTONOMOUS NAVIGATION METHODOLOGY

To achieve autonomous navigation, there are four steps that needs to happen in chronological order which are mapping, localization, path planning and low-level control. The following sub sections provide an overview of each technique applied. These techniques take advantage of the ROS network that was created in the previous section.

Mapping

Beginning with the first step which is to generate a map of the mobile platform's workspace. To do so, a Simultaneous Localization and Mapping (SLAM) algorithm known as FastSLAM 2.0 is applied. The fundamental workings of this algorithm are based on particle filters that recursively estimate a mobile robot's state and environment when only partial observations are made. FastSLAM 2.0 builds on top of the concepts established by FastSLAM 1.0 (Rao Blackwellization Filter SLAM [30]) by featuring two primary improvements which are first adding an improved proposal distribution and second, including an adaptive resampling method. The improved proposal distribution considers the measurements during sampling which enhances the accuracy since a precise sensor can be used to reduce the impact of noisy motion estimation. The adaptive resampling method also ensures proper number of samples are available to avoid particle depletion. This algorithm is implemented in ROS as GMapping which is an open source node that may be fitted within the environment that was created for the SECV.

Localization

Once a map is acquired, the next step is to estimate the SECV's pose within the map through localization algorithms. In this application, the wheel encoders and IMU are used to incrementally estimate the SECV's linear translation and angular displacement, respectively. This type of localization is known as dead reckoning and it is only feasible for short distance navigation as sensor drift accumulates and severely hinders the performance of localization. Revisiting Fig. 7, a custom localization node is created for the SECV to subscribe to the topics published by the encoders and IMU.

Path Planning

With the given map and localization complete, path planners are implemented to navigate the SECV from its initial location to the desired. To do so, a global planner known as Dijkstra's algorithm is implemented [31]. This planner is based on representing a map with nodes that are assigned values based on the cost of arriving. The goal of the algorithm is to find the shortest path between the starting and finishing node without colliding with any obstacles that were observed during the mapping process. Once a global planner has finished generating a path between the start and goal point, local path planners are responsible for considering real time sensor data to avoid collision with obstacles that were not present during the mapping phase. In this work, the Timed Elastic Band planner developed in [32] is implemented. This algorithm builds on top of the Elastic Band approach by considering an objective and cost function instead of forces that cause deformation to the bands [33]. This planner considers dynamic constraints of the mobile platform which the original Elastic Band planner did not. Additionally, an advantage of this planner is its ability to plan for all mobile robot drivetrain configurations such as differential, omnidirectional and Ackermann systems. The output of this algorithm is published to the cmd_vel topic as mentioned previously.

Low Level Control

The last step of the navigation procedure is to convert the output of the path planner in to meaningful commands for the driving and steering controllers. Beginning with driving, a software differential is implemented to account for the different turning circle diameters between the left and right wheels of the SECV. The following two equations describes the velocity differences based on the track width, linear and angular velocities. The intent is to improve maneuverability during cornering.

$$Right_{velocity} = v - (\dot{\theta} * t/2) \qquad (17)$$

$$Left_{velocity} = v + (\dot{\theta} * t/2) \qquad (18)$$

As previously mentioned, Fig. 9 illustrates the closed loop speed control block diagram with feedback from the wheel encoders. The error between the desired and actual velocity is processed

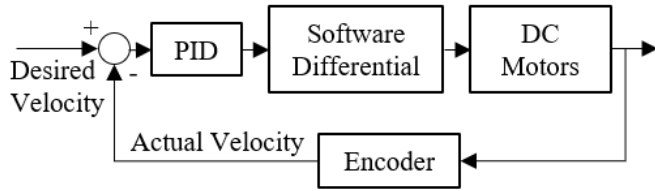by a PID controller which then takes advantage of the software differential before commanding the DC motors.

FIGURE 9. Closed Loop Speed Control

For steering, actuator stroke positions are mapped to steering angles experimentally with the physical prototype. The results are plotted and fitted with a third order line of best fit. The following two equations illustrates the actuator model which is used by a PID controller to control the steering as seen in Fig. 10.

$$Stroke_{left} = (5 * 10^{-5})\delta_L^3 + 0.0014\delta_L^2 - 0.7589\delta_L + 24.974 \quad (19)$$

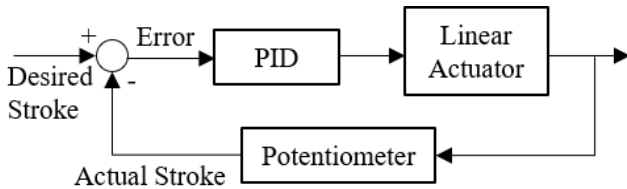$$Stroke_{right} = -(5 * 10^{-5})\delta_R^3 + 0.0014\delta_R^2 + 0.7586\delta_R + 24.974 \quad (20)$$

FIGURE 10. Closed Loop Stroke Position Control

RESULTS AND DISCUSSION

In this section, the proposed SECV prototype is subjected to various testing to assess its performance attributes and autonomous navigation abilities. For vehicle performance, attributes such as max speed, steering time and turning radius, are studied. These tests will provide a more in depth look at the capabilities of the prototype. Implementation of path planners with the onboard computer and sensors are also tested to evaluate its obstacle avoidance capability.

Vehicle Performance Test

Starting with vehicle performance tests which are intended to quantify the functionality and operational limits of the SECV. The results from the following series of tests are tabulated.

A. Max Speed

To find the maximum speed of the SECV, 5 tests over different distances are conducted. To account for acceleration time, each test is conducted with a five-meter head way to ensure the vehicle have reached top speed before entering the test. By timing the SECV over the 5 tests, the vehicle speed is calculated.

The following table summarizes the test results where the average max speed of the prototype is approximately 6.82 km/h which is a 10.73% difference when compared with the theoretical top speed value of 7.67 km/h. When considering the reaction time of the human operator during this test, this is an acceptable error percentage.

TABLE 1. Max Speed Results

Run	Distance (m)	Time (s)	Speed (km/h)
1	5	2.67	6.75
2	10	5.20	6.92
3	15	8.02	6.73
4	20	10.57	6.81
5	25	13.06	6.89
		Average	6.82

In terms of the steering response time, a test program that steers the wheels from full left to full right repeatedly is implemented. The program includes a timer that utilizes the potentiometer feedback from the linear actuators to determine the elapsed time to achieve full extension/retraction when connected with the wheel assembly in the SECV. The results over 5 cycles are shown below with each cycle being from one side to the other. The average steering time achieved is 0.9797 seconds which is faster than the required; thus, satisfiable.

TABLE 1. Steering Response Time Results

Run	Time (s)
1	0.9834
2	0.9652
3	0.9733
4	0.9863
5	0.9901
Average	0.9797

B. Minimum Turning Radius

The goal of this test is to evaluate both the steering system design as well as the lower controller on how close the results are to the theoretically calculated. To do this, three different steering configurations are selected; namely, Front Wheel Steer (axle 1 and 2), 4th Axle Steer (axle 1, 2, 4) and All Wheel Steer (all axles). Using Ackermann's steering geometry, the theoretical minimum turning radius based on maximum steering angle of 35 degrees is calculated. For experimental results, the SECV starts from rest with the maximum steering angles set. Since Ackermann geometry only holds for low speed cornering (which is classified as speeds lower than 30 km/h) [34] [35], the throttle is set to a constant scaled speed of 5 km/h in this test. The theoretical and experimental results from Front Wheel Steer (FWS), 4th Axle Steer (4AS), All Wheel Steer (AWS) are shown in the table below. When analyzing these values, it was found that the all steering configurations meet the theoretical value with negligible differences.

TABLE 6. Turning Radius Results

Steering Mode	Minimum Radius	Theoretical Radius	Error %
FWS	1.67 meters	1.62	3.09
4AS	1.41 meters	1.37	2.92
AWS	1.14 meters	1.08	5.56

Autonomous Navigation Test

In this section, the autonomous navigation ability of the SECV is experimentally tested. An obstacle that did not exist during the mapping phase is placed in between the SECV and its destination. As mentioned in the previous section, global and local path planners are implemented within the ROS network as illustrated by Fig. 7. The intent of the following is to evaluate both planner's ability to consider both the map and real time sensor data. Additionally, this will also test the lower controllers' ability to execute high-level plans accordingly.

A.   Experimental Setup

The base coordinate frame of the SECV is located at the bottom center of the chassis with the positive x axis (blue) and y axis (green) pointing forward and to the left, respectively, as seen in Fig. 11. An aluminum bridge is installed on top of the chassis to mount the laser scanner and IMU (a camera is included but not used here). Other hardware necessary for this test include the laptop, batteries, lower controllers and all the encoders for each wheel.
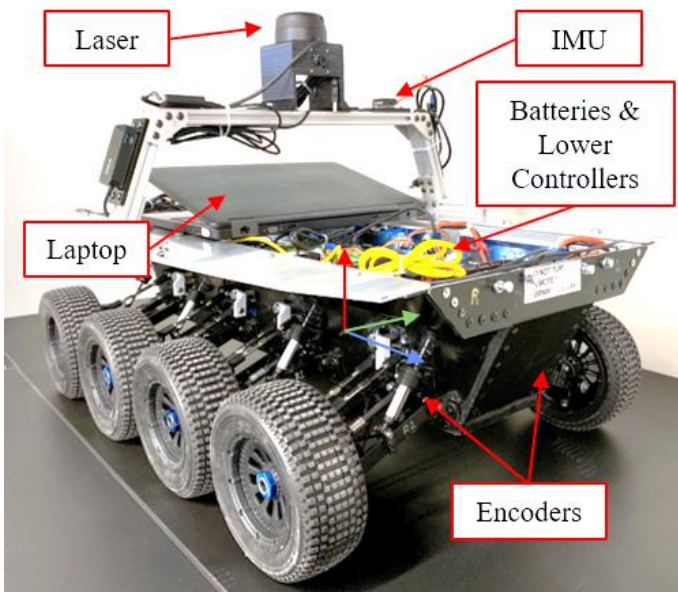

FIGURE 11. Experimental Setup (without aesthetic shell)

B.   Results

Based on the Performance Test section, the navigation tests are conducted with the AWS configuration since it offers the best cornering abilities. To start, the resultant trajectory generated by the path planners is as depicted in Fig. 12. As the SECV navigates, a cost map is updated with new sensor readings that consequently alters the local plan as the vehicle progresses. This behavior is noticeable around the 3-meter point where the SECV realized the obstacle is wider than previously anticipated, as a result re-corrected the heading angle to steer farther right. Moving forward, the maximum linear velocity of the SECV is set to 0.3 m/s for this experiment. In Fig. 13, the desired and actual velocities are shown to reach the set values. At around 11 and 24 seconds, the desired velocity decreased to just below 0.3 m/s as a result of computing hardware limitations. Based on the software differential as mentioned in the Low-Level Control section, the wheels on the left and right side of the vehicle experience different velocities to achieve better cornering maneuverability. This difference in velocity considers not only the linear velocity, but also the angular velocity which is presented in Fig. 14. In this figure, the desired and actual angular velocities are shown with more noise present in the latter. Based on the base coordinate frame assigned in the Experimental Setup section, a positive angular velocity implies a left turn and vice versa. The SECV began to steer right and away from the obstacle at around the 8 second mark. As the SECV passes the obstacle, it steers left and around behind the obstacle. Towards the end, the SECV steered back right just enough to correct its pose to be parallel with its initial orientation. Both the linear and angular velocities are given to the lower controller to calculate the desirable steering angles based on Ackermann geometry. The angles for only the front two axles are shown in Fig. 16 as the third and fourth axles are similar but in opposite directions. The physical experiment along with what the SECV perceives via its sensors are presented in Fig. 15.
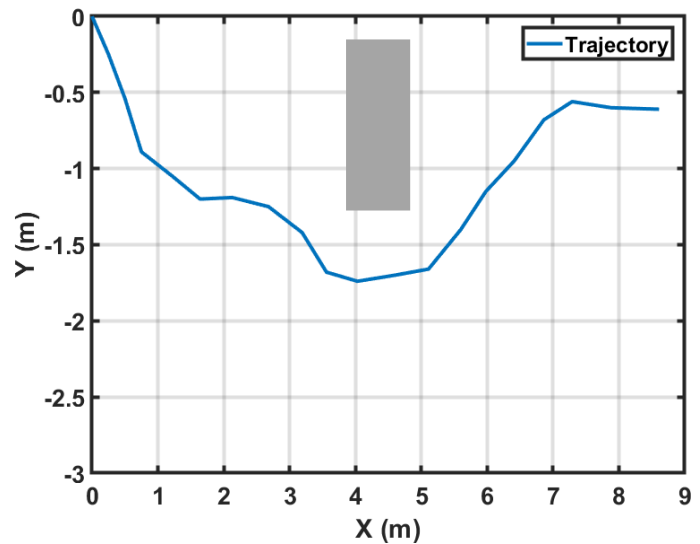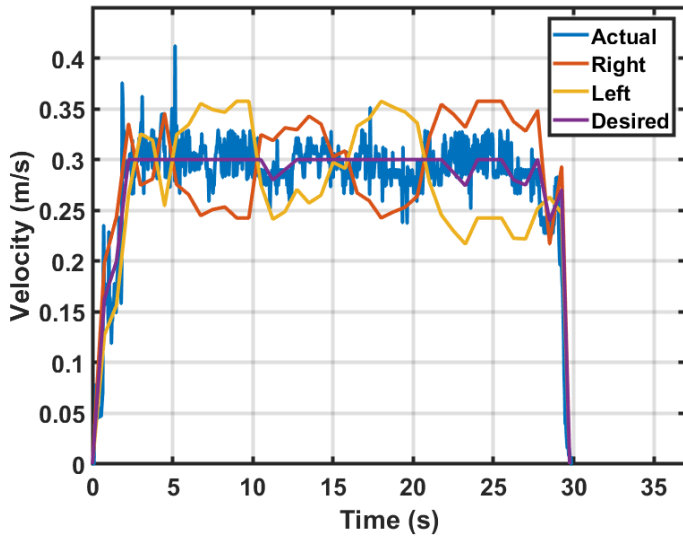

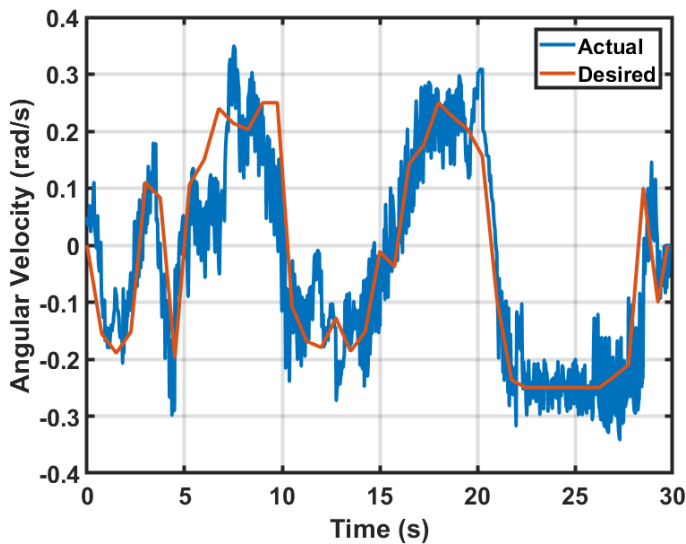**FIGURE 12.** SECV Trajectory

FIGURE 13. Linear Velocity
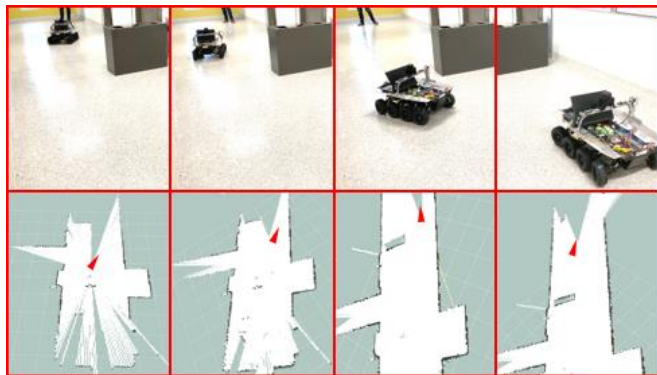

FIGURE 14. Angular Velocity

FIGURE 15. Physical Experiment (top), Data Visualization (bottom)
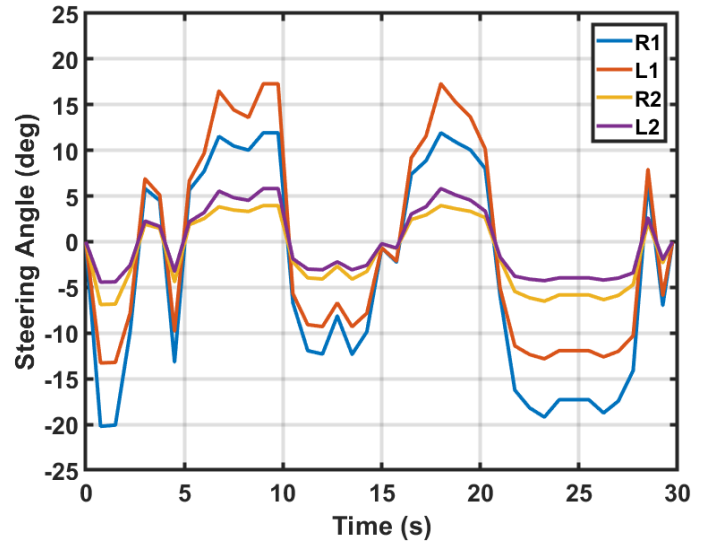

FIGURE 16. Steering Angles

CONCLUSION

In conclusion, this paper details the design and development of an autonomous multi-axle mobile platform that features independent steering. The goal is to create a 1:6 scaled robotic platform that mimics the design of a typical future multi-wheeled combat vehicle to create a tool for future autonomous vehicle research. More specifically, having this model allows for faster and more accessible tests, since the scaled model takes up far less space, weighs less, while all the steering geometry, suspension, and center of gravity is kept proportional. This makes the SECV a valid candidate when developing autonomous navigation algorithms for off road terrains and cluttered environments that are intended for its life size counterpart. To accomplish this, custom mechanical systems are designed from the ground up which entailed manufacturing and assembly of the suspension, chassis, driving and steering components. It is important to note that factors such as vibration and aerodynamics are negligible due to the scaled size. Electronics hardware including computing unit, sensors and actuators are successfully integrated within the vehicle while custom low-level software is created to form a complete development environment within ROS. The final platform is then subjected to vehicle performance testing to quantify its operational abilities and limits. With this knowledge, navigation algorithms that include mapping, localization and path planning are implemented and tested with physical experiment. The results from both types of testing validates the SECV as a fully functional prototype that yields a high potential for future autonomous navigation research. Going forward, all completed work based on the proposed platform will contribute to a more innovative future for the combat vehicle family.

ACKNOWLEDGEMENT

REFERENCES

[1] C. Army, "Light Armoured Vehicle (LAV) III," Government of Canada, 13 December 2017. [Online]. Available: http://www.army-armee.forces.gc.ca/en/vehicles/light-armoured-vehicle.page. [Accessed Janurary 2019].

[2] "LAV-25 Light Armoured Vehicle," Army Recognition, 27 September 2018. [Online]. Available: https://www.armyrecognition.com/us_army_wheeled_and_armoured_vehicle_uk/lav-25_8x8_light_armoured_vehicle_technical_data_sheet_specifications_pictures_video.html.

[3] "Light Armored Vehicles - LAV III APC," General Dynamics Land Systems, [Online]. Available: https://www.gdls.com/products/light-armored-vehicles/LAV-III-APC.html. [Accessed January 2019].

[4] "LAV III," General Dynamics Land Systems - Canada, [Online]. Available: https://www.gdlscanada.com/products/LAV/LAV-III.html. [Accessed January 2019].

[5] G. D. L. S. -. Canada, "LAV 6.0," A General Dynamics Business, [Online]. Available: https://www.gdlscanada.com/products/LAV/LAV-6.0.html. [Accessed January 2019].

[6] A. Genys, "LAV 700," Military-Today.com, [Online]. Available: http://www.military-today.com/apc/lav_700.htm. [Accessed January 2019].

[7] Q. Qiu, Z. Fan, Z. Meng, Q. Zhang, Y. Cong, B. Li, W. Ning and C. Zhao, "Extended Ackerman Steering Principle for the coordinated movement control of a four wheel drive agriculture mobile robot," *Computers and Electronics in Agriculture,* vol. 152, pp. 40-50, 2018.

[8] G. Kouros and L. Petrou, "PANDORA monstertruck: A 4WS4WD car-like robot for autonomous exploration in unknown environments," in *12th IEEE Conference on Industrial Electronics and Applications*, Siem Reap, Cambodia, 2017.

[9] T.-H. S. Li, M.-H. Lee, C.-W. Lin, G.-H. Liou and W.-C. Chen, "Design of Autonomous and Manual Driving System for 4WIS4WID Vehicle," *IEEE Access,* vol. 4, 2016.

[10] M. H. Ko, K. C. Kim, A. Suprem, N. P. Mahalik and B. S. Ryuh, "4WD mobile robot for autonomous steering using single camera based vision system," *International Journal of Intelligent Unmanned Systems,* vol. 2, no. 3, 2014.

[11] C.-J. Lin, S.-M. Hsiao, Y.-H. Wang, C.-H. Yeh, C.-F. Huang and T.-H. S. Li, "Design and implementation of a 4WS4WD mobile robot and its control applications," in *International Conference on System Science and Engineering*, Budapest, Hungary, 2013.

[12] H. Bo, "Precise navigation of a 4WS mobile robot," *Journal of Zhejiang University,* vol. 7, no. 2, pp. 185-193, 2006.

[13] C. Kim, A. M. Ashfaq, S. Kim, S. Back, Y. Kim, S. Hwang and J. Jang, "Motion Control of a 6WD/6WS wheeled platform with in-wheel motors to improve its maneuverability," *International Journal of Control, Automation and Systems,* vol. 13, no. 2, pp. 434-442, 2015.

[14] A. P. Aliseichik and V. E. Pavlovsky, "The model and dynamic estimates for the controllability and comfortability of a multiwheel mobile robot motion," *Automation and Remote Control,* vol. 76, no. 4, pp. 675-688, 2015.

[15] W. G. Kim, J. Y. Kang and K. Yi, "Drive control system design for stability and maneuverability of a 6WD/6WS vehicle," *International Journal of Automotive Technology,* vol. 12, no. 1, pp. 67-74, 2011.

[16] A. Mohamed, M. El-Gindy, J. Ren and H. Lang, "Optimal Collision-Free Path Planning for an Autonomous Multi-Wheeled Combat Vehicle," in *ASME International Design Engineering Technical Conferences and Computers and Information in Engineering Conference*, Cleveland, Ohio, 2017.

[17] P. D'Urso and M. El-Gindy, "Development of control strategies of a multi-wheeled combat vehicle," *International Journal of Automation and Control,* vol. 12, no. 3, 2018.

[18] A. Mohamed, M. El-Gindy and J. Ren, "Design and Performance Analysis of Robust H-infinity Controller for a Scaled Autonomous Multi-Wheeled Combat Vehicle Heading Control," in *ASME International Design Engineering Technical Conference & Computers and Information in Engineering Conference*, Quebec City, Canada, 2018.

[19] Military-Today, "Lav 6.0 Armored Personnel Carrier," Military-Today, [Online]. Available: http://www.military-today.com/apc/lav_6_0.htm. [Accessed April 2019].

[20] C. Robotics, "Husky: Unmanned Ground Vehicle," [Online]. Available: https://www.clearpathrobotics.com/husky-unmanned-ground-vehicle-robot/. [Accessed April 2019].

[21] J. G. Bralla, Design for Excellence, McGraw-Hill, 1996.

[22] "Friction and Automobile Tires," Hyper Physics, [Online]. Available: http://hyperphysics.phy-astr.gsu.edu/hbase/Mechanics/frictire.html. [Accessed April 2019].

[23] "Rolling Resistance," The Engineering ToolBox, 2008. [Online]. Available: https://www.engineeringtoolbox.com/rolling-friction-resistance-d_1303.html. [Accessed April 2019].

[24] R. G. Budynas and K. J. Nisbett, Shigley's Mechanical Engineering Design, New York: McGraw-Hill Education, 2015.

[25] K. J. Manner, "Fastener Handout - ME231," University of Wisconsin-Madison. [Online]. [Accessed 2017 November 2017].

[26] STock Drive Products / Sterling Instrument, "Technical Section Timing," [Online]. Available: http://www.sdp-si.com/PDFS/Technical-Section-Timing.pdf. [Accessed 22 November 2017].

[27] U.S. Navy Seabees, "Drive Lines, Differentials, Drive Axles, and Power Train Accessories," [Online]. Available: http://seabeemagazine.navylive.dodlive.mil/files/2014/0 5/14264A-Construction-Mechanic-Basic-Chapters-11.pdf. [Accessed 15 September 2017].

[28] Actuonix, "P16-P Linear Actuator with Feedback," Actuonix Motion Devices, [Online]. Available: https://www.actuonix.com/P16-P-Linear-Actuator-p/p16-p.htm. [Accessed April 2019].

[29] ROS, "About ROS," Open Source Robotics Foundation, [Online]. Available: http://www.ros.org/about-ros/. [Accessed Janurary 2019].

[30] G. Grisetti, G. D. Tipaldi, C. Stachniss, W. Burgard and D. Nardi, "Fast and accurate SLAM with Rao-Blackwellized particle filters," *Robotics and Autonomous Systems,* vol. 55, no. 1, pp. 30-38, 2007.

[31] E. W. Dijkstra, "A Note on Two Problems in Connexion with Graphs," *Numerische Mathematik,* vol. 1, pp. 269-271, 1959.

[32] C. Roesmann, T. Woesch, F. Hoffman and T. Bertram, "Trajectory modification considering dynamic constraints of autonomous robots," in *ROBOTIK 2012; 7th German Conference on Robotics*, Munich, Germany, 2012.

[33] O. Khatib and S. Quinlan, "Elastic bands: connecting path planning and control," in *IEEE International Conference on Robotics and Automation*, Atlanta, GA, 1993.

[34] J. Y. Wong, Theory of Ground Vehicles, Ottawa: John Wiley & Sons, Inc, 2008.

[35] O. M. o. Transportation, "Low Speed Vehicles," Ontario Government, 1 July 2017. [Online]. Available: http://www.mto.gov.on.ca/english/vehicles/low-speed-vehicles.shtml. [Accessed April 2019].